Cement and Concrete Composites 142 (2023) 105191

Contents lists available at ScienceDirect

Cement and Concrete Composites

journal homepage: www.elsevier.com/locate/cemconcomp

Investigation of the viscoelastic evolution of reactive magnesia cement pastes with accelerated hydration mechanisms

Yiming Peng [a], Cise Unluer [b,*]

[a] School of Engineering, University of Glasgow, Glasgow, G12 8LT, United Kingdom
[b] Department of Mechanical, Aerospace and Civil Engineering, University of Manchester, Manchester, M13 9PL, United Kingdom

ARTICLE INFO

Keywords:
Reactive magnesia cement
Hydration agents
Rheology
Viscoelasticity
Microstructure evolution

ABSTRACT

Viscoelasticity of reactive magnesia cement (RMC) pastes containing 3 different hydration agents (HCl, Mg$(CH_3COO)_2$ and $MgCl_2$) were investigated. Amplitude sweep, frequency sweep and time sweep of RMC pastes were examined within 3 h of hydration. Time-dependent evolution of storage modulus, loss modulus, phase angle, and shear stress were recorded. Measurements of pH, isothermal calorimetry, XRD, TG-DTG and FTIR were used to analyze hydration reaction and products. Addition of hydration agents (HAs) accelerated the growth rate of storage modulus/loss modulus over time. $MgCl_2$ demonstrated the greatest acceleration influence, also reflected in non-destructive structural build-up and buildability related to 3D printing applications. Addition of $MgCl_2$ and HCl advanced the initial setting time of RMC pastes to 100–110 min, during which yield stress reached maximum, and decreased afterwards. Within 3 h of hydration, pastes containing $MgCl_2$ revealed lowest pH, highest heat release and brucite concentration. HAs inclusion precipitated brucite away from MgO particles in the bulk solution, creating a bridge between MgO particles and enabling denser microscopic network structure.

1. Introduction

Portland cement (PC), the most commonly used building material, requires significant resource, energy and carbon dioxide (CO_2) to be produced. Currently, PC production exceeds 4 billion tons each year [1,2], and the CO_2 generated during this process accounts for ~8% of worldwide anthropogenic CO_2 emissions [3]. To address this issue, research initiatives are focusing on the development of alternative cementitious materials with potentially lower environmental impacts, including alkali-activated materials, geopolymers [4,5], magnesia-based cements [6,7], and limestone calcined clay (LC^3) [8]. Among these, carbonated reactive magnesia cement (RMC) is a possible candidate due to its strength gain mechanism that is linked with CO_2 sequestration [9–12]. Within this system, the primary raw ingredient, light-burned magnesia (MgO), has a much lower calcination temperature (750 °C vs. 1400 °C) than PC [13] and can also be obtained from industrial by-products such as reject brine [14,15]. Finally, the final carbonation products that form in carbonated RMC systems, hydrated magnesium carbonates (HMCs), can convert back to RMC through thermal decomposition [7], enabling the complete recycling of these mixes at the end of their lifetime [16].

The reaction mechanisms of RMC system involve a few steps that initiates with the release of OH^- upon the contact of MgO with water. Once the ion concentration approaches supersaturation, brucite precipitates on the surface of MgO particles, therefore slowing and inhibiting the subsequent hydration process [17–19]. The pH value of the solution steadily increases throughout this procedure [20]. When the right conditions are provided, the carbonation of brucite provides significant strength gain in RMC mixes [21,22]. During carbonation, brucite and dissolved CO_2 progressively transform into HMCs, producing a denser and strong network structure. The reduction in the porosity of RMC concrete with curing duration results in a higher mechanical performance [23–25].

In addition to the optimization of carbonation conditions [11,26], some studies have looked into the use of different hydration agents (HAs) as a solution to the inherently low dissolution of MgO [23], hence accelerating the hydration reaction, increasing the formation of brucite and subsequent HMCs, and thereby enhancing strength [19,27]. Several different additives have been proposed, including magnesium acetate ($Mg(CH_3COO)_2$), magnesium chloride ($MgCl_2$), and hydrochloric acid (HCl) [28–31]. HCl can be used to facilitate the dissolution of brucite deposited on the surface of MgO particles, hence increasing the

* Corresponding author.
E-mail address: cise.unluer@manchester.ac.uk (C. Unluer).

https://doi.org/10.1016/j.cemconcomp.2023.105191
Received 5 January 2023; Received in revised form 28 May 2023; Accepted 21 June 2023
Available online 21 June 2023

hydration degree of MgO. Alternatively, $Mg(CH_3COO)_2$ and $MgCl_2$ demonstrated comparable approaches in promoting the hydration process. In RMC pastes containing $Mg(CH_3COO)_2$, the dissolved Mg^{2+} from MgO particles leaves the original particles and nucleates at new sites. Dung et al. [27] discovered that the introduction of $Mg(CH_3COO)_2$ greatly increases the degree of hydration and carbonation, resulting in an improvement in mechanical strength.

While several studies have been conducted on the curing conditions, reaction mechanisms and mechanical properties of RMC systems, their rheological characteristics have yet to be discovered. Fresh-state cement pastes are typically plastic owing to their suspension feature. As time passes and the hydration process continues, the proportion of elastic components in cement steadily increases until it loses its fluidity, proving the intrinsic property of viscoelasticity [32]. The optimization and regulation of the rheological behavior of cement systems is critical as it plays a key role in establishing a theoretical and practical foundation for the fabrication of robust structures through emerging technologies such as 3D printing [33–36]. Accordingly, the requirements of 3D printing process for building materials include reasonable thixotropy and buildability [37–41]. Previous studies [42–44] have successfully used RMC-based binder as a raw material in the development of 3D printed structures, demonstrating the viability of attaining the required thixotropy and buildability in mixes involving RMC.

Considering the lack studies on the time-dependent rheo-viscoelastic properties of RMC systems, this study aims to fill this gap in the literature by utilizing small amplitude oscillation shear (SAOS) to characterize the viscoelasticity of fresh RMC pastes mixed with various HAs. During this process, the storage modulus, loss modulus, phase angle, and shear stress were set as the primary parameters. Along with viscoelastic characterization, hydration kinetics, X-ray diffraction (XRD), thermogravimetry analysis (TGA) and Fourier transform infrared spectroscopy (FTIR) were employed to determine the reaction rate and degree of RMC at different durations. Keeping in mind that rheological properties are the most essential and precise quantitative indicators for the workability of 3D printing materials [33], the results generated by this study can provide a detailed theoretical and experimental basis for the application of RMC systems in the field of 3D printing, during which HAs can effectively improve the early-stage buildability of RMC. These findings can serve as a key guide for the rheology of RMC mixes during their extrusion from a 3D printer nozzle and subsequent non-destructive structural build-up on a platform.

2. Materials and methodology

2.1. Materials and mix proportions

The raw material used in this study was reactive magnesia provided by Richard Baker Harrison (UK), and its chemical composition and particle size distribution is shown in Table 1 and Fig. 1 respectively. Three different HAs, i.e. HCl, $Mg(CH_3COO)_2$ and $MgCl_2$, provided by Sigma-Aldrich were used to promote the hydration of RMC mixes.

The mix proportions used in this study are shown in Table 2. The water-to-binder ratio (w/b) of each group was kept constant at 0.6. In addition to the first reference sample, three kinds of HA with the same molar concentration (0.1 M) were added to investigate the hydration mechanism of each paste, respectively. The mixing stage was to dissolve HA in water, thoroughly mix, and then rest for 10 min to completely balance the exothermic action of the dissolved HA. The solution was then mixed with MgO clinker and stirred for 5 min.

Table 1
Chemical composition of RMC.

Chemical composition								LOI
MgO	SiO_2	CaO	Al_2O_3	Fe_2O_3	Na_2O	P_2O_5	SO_3	
88.9	2.86	2.23	0.63	0.90	0.15	0.18	0.28	3.6

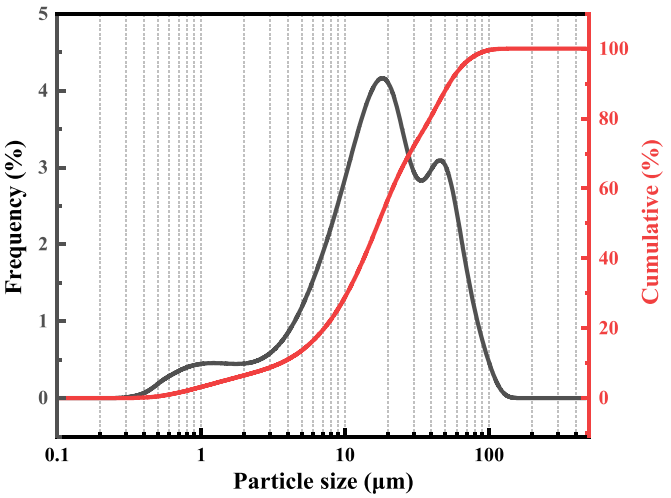

Fig. 1. Particle size distribution of RMC.

Table 2
Mix proportions used in this study.

Mix label	MgO (g)	H_2O (g)	HA solution	
			Type	Concentration (M)
MgO-H_2O	100	60	H_2O	–
MgO-HCl0.1	100	60	HCl	0.1
MgO-MCH0.1	100	60	$Mg(CH_3COO)_2$	0.1
MgO-MCl0.1	100	60	$MgCl_2$	0.1

2.2. Viscoelasticity measurement

The rheometer used in this study was an Anton Paar MCR 302. The test rotor of rheometer is a coaxial cylinder, with an inner diameter and an outer diameter of 26.660 mm and 28.915 mm respectively. Considering the fact that when the rotor begins to spin from a static position, wall slip between the smooth inner wall of the rotor and paste may occur [45]. To minimize the inaccuracy caused by this phenomenon, a serrated-surfaced cylinder was selected for the rheological test. Each set of samples was pre-sheared with the shear rate of 40 s^{-1} for 60 s before the test. Mineral oil was evenly dropped on the sample surface during all testing processes to prevent the water in RMC paste from volatilizing.

To characterize the viscoelastic evolution of fresh RMC system more precisely, the linear viscoelastic region (LVR) that maintains the paste in a non-destructive condition should first be determined [46–48]. The amplitude and frequency sweep test protocols utilized in this study are shown in Fig. 2. The amplitude sweep test consisted of a total of 21 test points with a time interval of 15 s between each point. Maintaining a 1 Hz oscillation frequency, the strain grew logarithmically from 0.001% to 10%. The frequency sweep used the 0.006% (i.e. LVR critical strain) acquired from the amplitude sweep as the constant strain value and the frequency was reduced from 100 Hz to 0.1 Hz.

After obtaining a reasonable amplitude and frequency, a time sweep was applied to each sample. To completely investigate the viscoelastic evolution difference across RMC systems incorporating different HA, each group was tested for up to 3 h, with a test point recorded every 10 s. The storage modulus G', loss modulus G'', phase angle δ, and the shear stress τ were all included in the test parameters.

2.3. Hydration stoppage

The hydration of samples with resting time of 1 h, 2 h and 3 h were terminated respectively. Firstly, 3 g of fresh sample was taken and

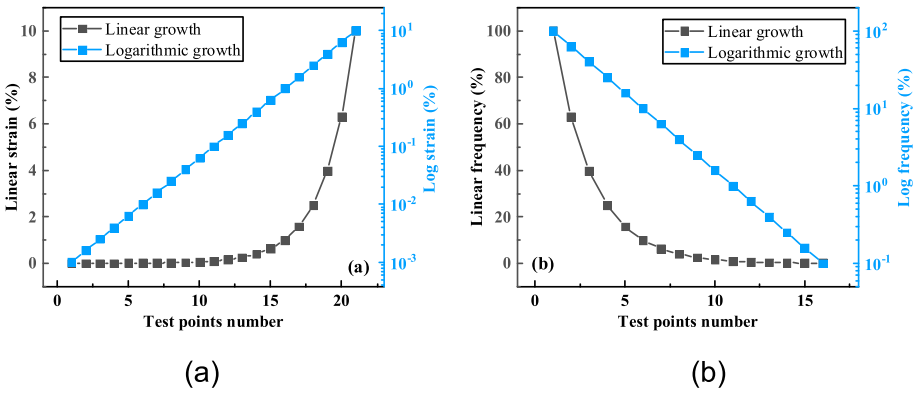

Fig. 2. Rheological protocol for viscoelastic measurements, showing: (a) Amplitude sweep and (b) frequency sweep.

approximately 100 ml isopropanol was poured into the beaker. After mixing for 10 min, at which point samples precipitated at the bottom of the beaker, the isopropanol was poured out from the upper layer and each sample was placed on filter paper for filtration. Then each sample was washed by using acetone again and placed in the drying oven for 24 h at a temperature of 60 °C. After drying them completely, each sample was thoroughly ground by using a mortar and pestle for microscopic analysis preparation.

2.4. Microstructure analysis

SevenCompact pH meter S210 was used for pH measurement. Prior to testing, the instrument was calibrated using a standard solution. After completely mixing MgO with water or the solution containing HA, the probe was inserted into the paste every 30 min for measurement. The pH value was recorded after the device remained stable. Each test was repeated three times, and their average values were taken for the final results.

The heat of hydration up to 48 h was determined using an I-Cal 4000 HPC isothermal calorimeter. The test temperature stayed constant at 20 °C. Each sample contained 50 g of RMC and 30 g of water. Since the RMC hydration exothermic peak was concentrated in the stage of initial dissolving, each point was measured every 10 s for the first 40 min and then every 60 s for the remaining duration.

The sample XRD was tested by a Miniflex Benchtop X-ray diffractometer with advanced detector. The range of 2θ was 5–80°, scan step was 0.02°, and scan speed was 5°/min. ZnO at 20 wt% was used as an internal standard, and X'Pert HighScore Plus 3.0 was used for Rietveld quantitative analysis of the data.

A Perkin Elmer TGA 8000 was used to conduct the thermogravimetric analysis. Each batch of sample weighed between 30 mg and 40 mg. The sample temperature was maintained at 30 °C initially and heated to 1000 °C at a rate of 10 °C/min. The FTIR spectra of the samples were carried out by a Perkin Elmer FTIR Spectrometer, with the wavenumber range of 4000 cm^{-1} - 3500 cm^{-1} for the purpose of analyzing -OH stretching band. The test results for each sample were the average of eight scans.

3. Results

3.1. Viscoelastic behavior

The strain sweep and frequency sweep curves for fresh RMC pastes are shown in Fig. 3. As shown in Fig. 3(a), the G' and G'' stayed stable when the strain value was less than approximately 10^{-2}%. Within this range, the paste was LVR-compliant and exhibited solid-like features. When the strain value exceeded this range, the two moduli began to decrease significantly and eventually intersected at a point commonly referred to as the flow point. The observation that the fraction of loss modulus G'' exceeded G' indicated that the paste converted to a liquid and flowed readily macroscopically. When performing oscillatory tests, a high oscillation frequency indicated a higher shear rate of inner cylinder. At this stage, no amount of strain could completely release the stress [47,49]. As shown in Fig. 3(b), when the frequency was larger than 1 Hz, the fluctuation extent of the loss modulus was considerable, implying that an oscillatory frequency that was too rapid might cause the test results to be delayed. When the frequency was steadily reduced to 0.1 Hz, the two moduli, particularly G', dramatically diminished, which might result in shear thinning owing to oscillatory shear at high speeds. As a consequence of these two tests, 0.001% and 1 Hz were selected as constant amplitude and frequency values to complete the subsequent test without disturbing the paste microstructure.

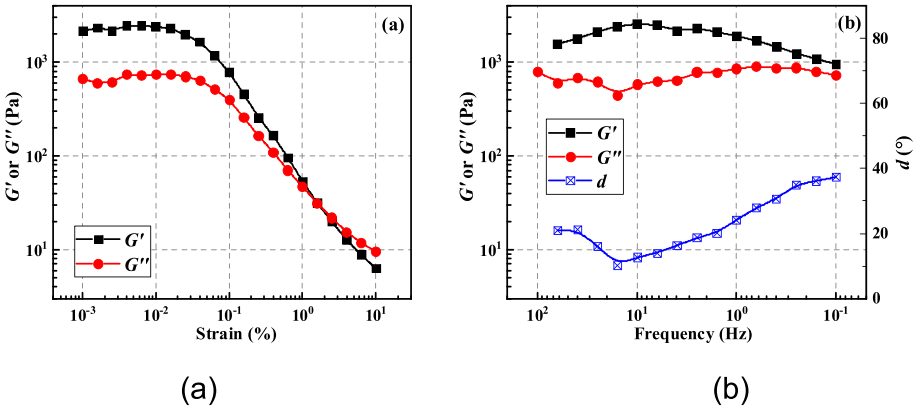

Fig. 3. Typical curves of RMC pastes without the incorporation of HAs, showing: (a) Amplitude sweep and (b) frequency sweep.

Fig. 4 illustrates the time sweep outcomes of the tested samples with constant strain and amplitude. In comparison to the findings obtained with PC clinker [50,51], the test points for these four RMC pastes fluctuated significantly. The G' and G'' of reference paste, i.e. without HA were the lowest among the four groups when hydrated for the same time. The increase trend of two moduli with the addition of 0.1 M Mg $(CH_3COO)_2$ over time was the most similar to that of the reference sample, with approximately the same growth rate when the ordinates were given in logarithm. In contrast to the above two samples, the pastes containing HCl and $MgCl_2$ exhibited a quick rise in G' and G'' within 100 min. The G' of MgO-HCl0.1 climbed from 10^4 Pa to around 10^7 Pa over this period, whilst the samples incorporating $MgCl_2$ grew slowly owing to its highest initial modulus. It should be noted that when the elapsed time surpassed approximately 110 min, the rheometer was unable to measure the G'' of samples containing HCl and $MgCl_2$, and their G' would not continue to increase but will remain stable instead. This showed that the two groups of pastes had been in the initial setting stage, so the subsequent test results would not be further analyzed. Compared with these two moduli, the phase angle exhibited a larger degree of fluctuation.

Besides the storage and loss moduli, the shear stress recorded from rheometer was measured as well during SAOS (Fig. 5). As with the growth pattern of G', the shear stress exhibited a roughly exponential development with time. The reference sample and the paste containing $Mg(CH_3COO)_2$ had a much smaller growth rate than the other two samples. By amplification of the black and blue curves in Fig. 5, it can be found that the shear stress of paste added with $Mg(CH_3COO)_2$ was more than 5 times that of reference paste at 180 min. The former had a stress value of 34.7 Pa, while the latter had a value of 7.93 Pa. The shear stress of MgO-HCl0.1 and MgO-MCl0.1 exhibited a peak with a same position

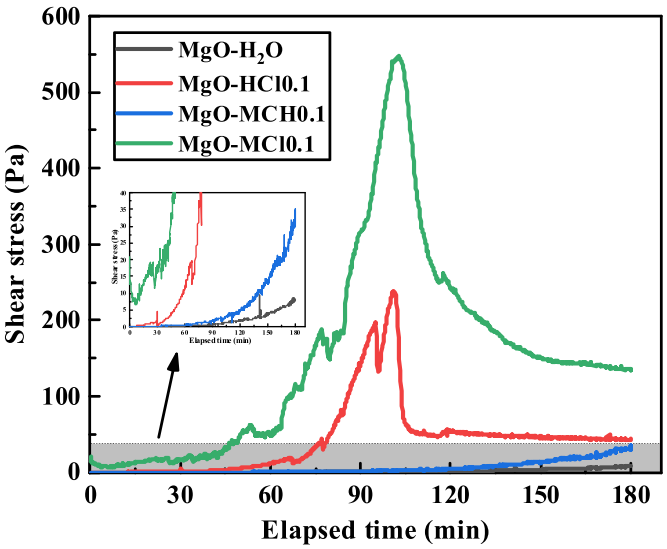

Fig. 5. Shear stress evolutions of RMC pastes.

that corresponded to their storage modulus. The highest value of MgO-HCl0.1 sample was 238 Pa at 101 min, whereas MgO-MCl0.1 sample had a peak value of 547 Pa at 103 min. It is usually considered that time sweep with tiny strain have little effect on the microstructure of measured sample [52]. Although the rheometer cylinder applied a much smaller amplitude than the LVR critical amplitude of RMC paste during the measurement, due to the long duration of the action, once the effect of the alternating stress accumulated to a certain extent, the yield stress

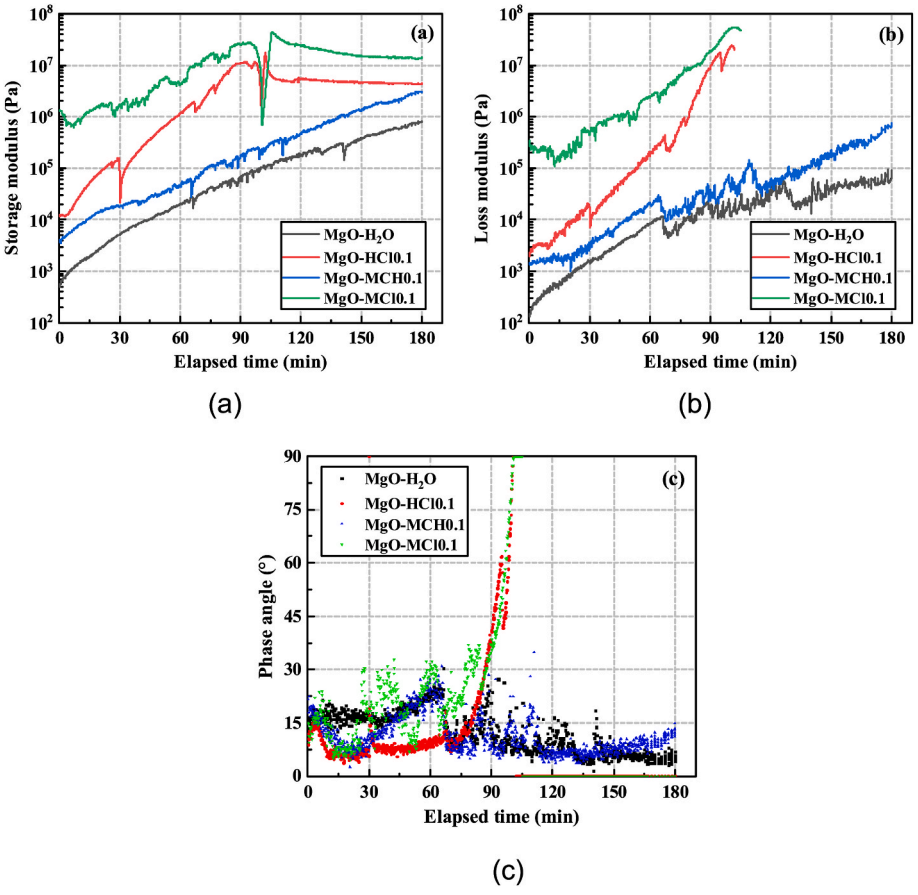

Fig. 4. Evolution of viscoelastic parameters with elapsed time in RMC pastes containing different HAs, showing: (a) G' evolution, (b) G'' evolution, and (c) phase angle δ.

in these two pastes would decrease significantly after reaching a peak, which was similar to material fatigue failure. Since the *G'* growth rate, i.e. the structural build-up rate, of MgO-H_2O and MgO-MCH0.1 was slow with time, and their corresponding peaks did not arrive within 180 min, their test curves did not exhibit the same change trend as the previous two pastes.

As observed in these rheo-viscoelastic behaviors, the primary impact of HAs on RMC pastes in the early stage was to increase their storage modulus, static yield stress and their evolution speed. The corresponding 3D printing stage closely connected to these two parameters involves the non-destructive structural build-up process of extruding the material from the nozzle and shaping it on the platform. After the material is deposited on the platform, the previously extruded lower layers are gradually subjected to the gravity of the upper layers. To avoid the deformation of the extruded structure, the static yield stress of the lower layers must demonstrate a greater rate of increase than the extrusion stress imposed by the upper layers during the printing process [38]. The addition of HAs (particularly $MgCl_2$ and HCl) may significantly enhance the structural build-up rate and early strength of RMC mixes, which is crucial for their buildability. However, considering that RMC mixes containing HAs demonstrated an initial setting time of around 100 min, their open time would be limited. Therefore, it is important to establish a balance between the duration required for maintaining the desired workability and buildability of RMC systems.

3.2. pH

The pH values of four samples taken within 180 min after hydration are shown in Fig. 6. All the tests were performed every 30 min. It can be found that the pH value of MgO-H_2O was the highest, reaching 12.72 at 30 min. As time passed, its pH value progressively declined to 12.5 in 180 min. Furthermore, when HAs were added, the pH value of pastes all declined dramatically. The pH value of paste decreased to about 10 after incorporating 0.1 M $MgCl_2$, while the pH values of MgO-HCl and MgO-MCH were almost equal. In contrast to the reference sample, the pH of pastes containing HA steadily increased over time.

According to the prior research [53], when magnesium oxide combines with water, the resulting paste solution is composed of Mg^{2+}, OH^-, and $Mg(OH)_2$. In principle, due to the limited solubility of brucite, the pH of paste solution will be only 10.5. However, due to the inclusion of a small amount of calcium oxide in RMC clinker, the OH^- concentration will significantly increase and results in the highest pH value of control sample. Due to the acidity of $Mg(CH_3COO)_2$ and HCl aqueous solutions, their addition will consume OH^- in the solution, thus lowering the pH. The mechanism of RMC incorporating $MgCl_2$ is more similar to that of magnesium oxychloride cement. When the concentrations of Mg^{2+} and OH^- are progressively increased, the formation of $[Mg_x(OH)_y(H_2O)_z]^{2x-y}$ is promoted, dramatically decreasing the concentration of OH^- in the solution [54].

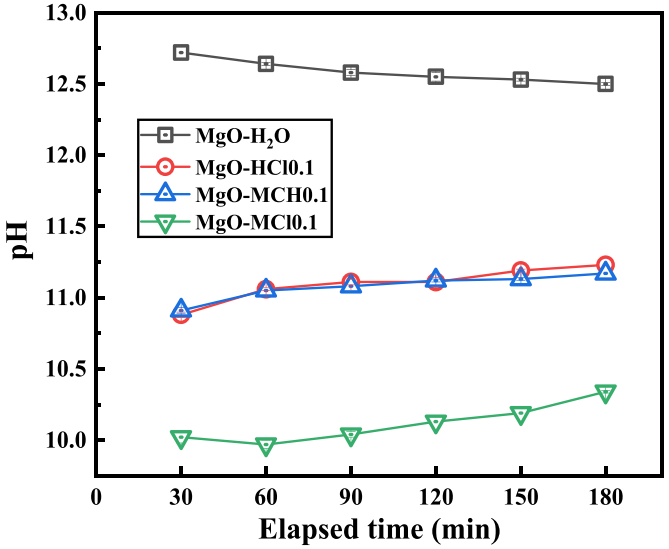

Fig. 6. pH values of selected RMC pastes.

3.3. Hydration

Fig. 7(a) and (b) show the heat flow and cumulative heat release of RMC pastes after 3 h of hydration, respectively, and their sub-figures also illustrate the data up to 48 h. All samples were mixed for 2 min to ensure that the first exothermic peak was not missed during measurement. As seen in Fig. 7(a), the difference in the heat flow curves of the four mix proportions was relatively modest throughout the first 3 h. The exothermic rate reached the maximum at approximately 10 min after adding HCl, followed by MgO-MCl0.1. When hydration was continued, the heat flow, as well as cumulative heat release (Fig. 7(b)), of MgO-MCl0.1 was remarkably larger than that of the other three samples. At the conclusion of 3 h, the total heat released of MgO-MCl0.1 was 52.3 J/g, while the total heat released by the other three groups was between 40.6 and 41.4 J/g. When the hydration period was increased from 3 h to 48 h, the heat flow of paste containing $MgCl_2$ exhibited a more significant sub-peak at 4 h than that of the other groups. After 12 h of hydration, the heat flow of MgO-MCl0.1 progressively declined until it was similar to the rest samples, which was consistent with prior observations [31].

3.4. XRD

Fig. 8 shows the XRD patterns of hydration for 1 h, 2 h and 3 h respectively. Qualitative analysis of phase composition revealed that fresh RMC mixes were mostly composed of four products: periclase (MgO; ICSD#173128), brucite ($Mg(OH)_2$; ICSD#34401), silicon oxide (SiO_2; ICSD#27833), and calcium carbonate ($CaCO_3$; ICSD#158258), in which a small quantity of SiO_2 and $CaCO_3$ were derived from the basic material RMC. With the progress of hydration process, the peak of periclase (37.1°, 43.1° and 62.5° 2θ) decreased regardless of HAs' presence. Meanwhile, the peak of brucite (18.5°, 38.1°, 51.0° and 58.8° 2θ) gradually increased, which could be proven quantitatively by using Rietveld analysis shown in Table 3.

After 1 h of hydration, the mass percentage of brucite in the sample was only 21.8%, while the content of brucite rose to 27.3% at 3 h. At 1 h, paste containing 0.1 M $Mg(CH_3COO)_2$ produced the most brucite (26.2%). However, MgO-MCl0.1 had the highest brucite concentration at 3 h, reaching 31%. The brucite content of RMC pastes containing HAs at 3 h was 2.5–3.7% higher than that of the reference sample, showing that HAs played an important role in accelerating the hydration of RMC. With the addition of HAs, brucite originally covering the surface of MgO particles was further dissolved, resulting in the precipitation of Mg^{2+} away from the original nucleation particles. This enabled the densification of the microstructure within the fresh RMC paste [30], causing its viscoelasticity (i.e. particularly the storage modulus representing elastic properties) to rapidly increase.

3.5. TG-DTG

To determine the fraction of hydrate components generated during viscoelasticity evaluation, the TG and DTG of the four pastes as a function of temperature after termination of hydration and complete drying were analyzed, as shown in Fig. 9. Due to the absence of carbonation products (HMCs) in fresh RMC paste, the main weight loss between 300 °C and 500 °C corresponds to the non-carbonated brucite decomposes into periclase [23,25]. By further analyzing the mass loss in this interval, the results in Fig. 10 could be obtained. The weight loss percentage of each samples rose when the hydration time was increased.

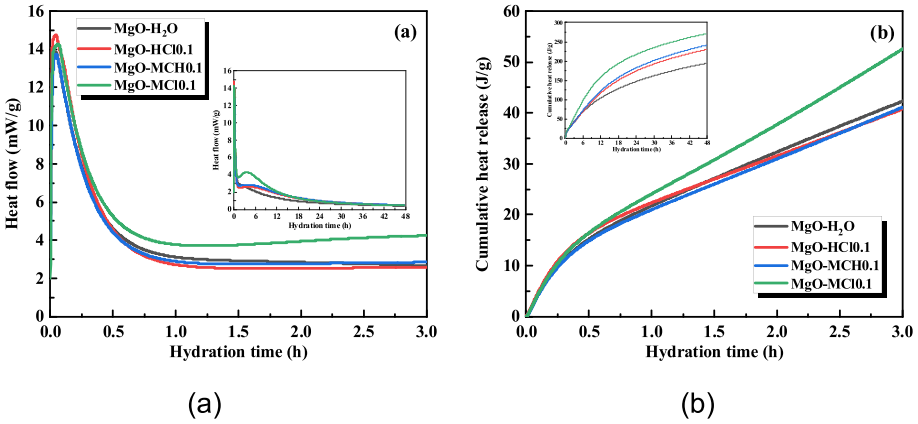

Fig. 7. Isothermal calorimetry results of RMC pastes, showing: (a) Heat flow and (b) cumulative heat release.

For the same hydration time, the weight loss of the sample without HA was the least, while the sample incorporating 0.1 M $MgCl_2$ displayed the largest weight loss, peaking at 11.07% after 3 h of hydration. When the temperature was between 50 °C and 300 °C, the mass loss was proportional to the decomposition of bound water [31]. At around 600 °C, a minor peak occurred in the DTG curve due to the decarbonation of a trace quantity of magnesite in the raw material (RMC) [23,55]. The results presented in this section demonstrated that the addition of HA accelerated the hydration process and promoted brucite formation, thus densifying the early microstructure of RMC system and contributing to the evolution of *G'*.

3.6. FTIR

The FTIR spectra of fresh RMC pastes with and without HA are shown in Fig. 11. A wavenumber range of 4000 cm^{-1} to 3500 cm^{-1} was selected since there were no carbonation products in the fresh RMC pastes and only a certain amount of brucite was formed, allowing just the -OH stretching band to be observed [27]. At varying hydration durations, each group of paste had a clear and distinctive absorption peak at 3690 cm^{-1}, which correlated to the presence of brucite. The absorption peak of -OH became more pronounced with hydration time, indicating that the formation of brucite increased steadily as hydration advanced. After 2 h of hydration, the absorption peak of the pastes containing HAs became significantly greater than that of the control group. The characteristic peak amplitude associated with the paste containing $MgCl_2$ was the greatest, which was consistent with the prior quantitative XRD and DTG results.

4. Discussion

The results of the rheological and microscopic analysis presented above demonstrated that the addition of HAs not only significantly improved the initial storage modulus of MgO-H_2O mixtures, but also accelerated the growth rate of both *G'* and *G''* over time. It was particularly notable that the *G''* of RMC pastes incorporating HCl and $MgCl_2$ could not be measured after the hydration time exceeded 110 min, suggesting the initiation of the first setting stage. Meanwhile, *G'* increased from the order of 10^3–10^6 Pa in the reference sample after 180 min, whereas *G"* increased from 10^2 to 10^5 Pa. The viscous and elastic behavior demonstrated by the MgO-H_2O system after 3 h of hydration indicated that the paste did not achieve its initial setting condition.

According to the reaction process proposed by previous studies [30,31], the addition of HCl increases the concentration of H^+ in cement suspension, during which the free H^+ rapidly diffuses on the surfaces of MgO solid particles and undergoes chemical reaction, as shown in Eq. (1). This is followed by the formation of brucite with Mg^{2+} and OH^- in the bulk solution. The optimization of this reaction mechanism improves the space for the further hydration of MgO.

$$MgO_{(s)} + 2H^+_{(aq)} \rightarrow Mg^{2+}_{(aq)} + H_2O_{(l)} \quad (1)$$

Similarly, the hydration mechanism of MgO changed after the addition of $Mg(CH_3COO)_2$ and $MgCl_2$. Taking $Mg(CH_3COO)_2$ as an example, its incorporation enabled the dissolution of Mg^{2+} on the surface of MgO particles away from the original reaction particles, followed by its reaction with OH^- to form brucite in the bulk solution [28]. The corresponding reaction mechanism is shown in Eqs. (2)–(5):

Dissociation of Magnesium acetate:

$$Mg(CH_3COO)_{2(aq)} \rightarrow 2CH_3COO^-{}_{(aq)} + Mg^{2+}{}_{(aq)} \quad (2)$$

Dissolution of periclase:

$$MgO_{(s)} + CH_3COO^-{}_{(aq)} + H_2O_{(l)} \rightarrow CH_3COOMg^+{}_{(aq)} + 2OH^-{}_{(aq)} \quad (3)$$

Dissociation of magnesium and acetate ions:

$$CH_3COOMg^+{}_{(aq)} \rightarrow CH_3COO^-{}_{(aq)} + Mg^{2+}{}_{(aq)} \quad (4)$$

Brucite precipitates due to supersaturation:

$$Mg^{2+}{}_{(aq)} + 2OH^-{}_{(aq)} \rightarrow Mg(OH)_{2(s)} \quad (5)$$

The findings obtained in this study indicated that the primary mechanism of HAs involved the relocation of Mg^{2+} away from the original MgO particles and the formation of $Mg(OH)_2$ in the bulk solution. This mechanism not only alleviated the blocking effect of $Mg(OH)_2$ on hydration due to its wrapping on the surface of MgO particles, but also formed a network between MgO and $Mg(OH)_2$ particles, resulting in a significant improvement in the storage modulus of RMC pastes. As seen in Fig. 12, without the addition of HA, MgO-H_2O suspension mostly consisted of MgO, $Mg(OH)_2$ wrapped on the surface of MgO particles and $Mg(OH)_2$ suspended in the bulk solution. Due to the high specific surface area of MgO particles, they could create flocculation structures as those observed between PC particles, thereby wrapping some of the available water and preventing it from flowing freely. Because the concentration of free Mg^{2+} in the bulk solution significantly increased with the addition of HAs, more $Mg(OH)_2$ was produced in the solution.

In the case of PC mixes, when water and cement clinker are fully and evenly mixed, cement particles quickly form flocculation structures and early hydration products are generated predominantly at the contact points of the flocculation particles [56]. Analogously, brucite is also formed between the flocculation structure and MgO particles wrapped in $Mg(OH)_2$, as shown in Fig. 12(b). This is a similar mechanism to the bridge provided by C-S-H that gradually connects PC particles together and promotes the development of a micro-network structure, thereby improving the ability of the cement paste to resist external shear action [57,58]. Accordingly, the addition of HAs not only improved the storage

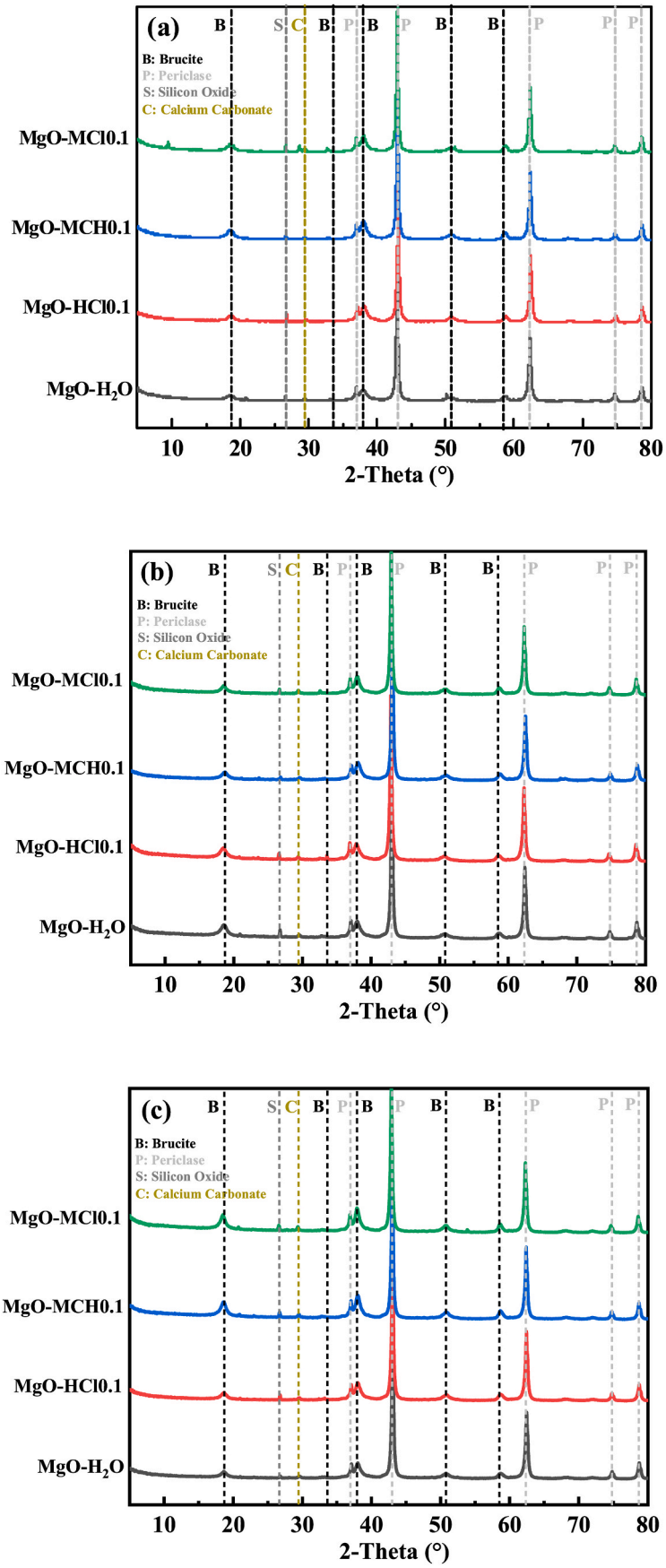

Fig. 8. XRD analysis of RMC pastes after hydration durations of: (a) 1 h, (b) 2 h, and (c) 3 h.

Table 3
Phase compositions in RMC mixes, calculated by XRD Rietveld analysis.

Sample	1 h		2 h		3 h	
	MgO	$Mg(OH)_2$	MgO	$Mg(OH)_2$	MgO	$Mg(OH)_2$
MgO-H_2O	77.6	21.8	76.5	22.5	71.7	27.3
MgO-HCl0.1	73.9	24.8	73.7	25.3	69.3	29.8
MgO-MCH0.1	73.1	26.2	69.9	29.2	68.6	30.4
MgO-MCl0.1	73.9	24.9	72.8	25.7	67.8	31

modulus of RMC pastes at the initial stage of mixing, but also accelerated the development of the microstructure in the first several hours.

A comparison of the three types of HAs used in this study revealed that $MgCl_2$ had the greatest effect on the development of the *G'*, i.e., structural build-up, followed by HCl. Through microscopic analysis, the distinctions in the effects of various HAs on the fresh RMC system were verified. The results of isothermal calorimetry demonstrated that the RMC system containing $MgCl_2$ had the greatest hydration rate. In addition, XRD, TG, and FTIR indicated that the addition of $MgCl_2$ and HCl (particularly $MgCl_2$) accelerated the formation of brucite and densified the early microstructure, thereby enhancing the resistance of fresh pastes to external shear forces, which was consistent with the viscoelastic measurement results.

This study successfully determined the optimum HA for the freshly mixed RMC system by means of experimental exploration and uncovered the underlying mechanism of change. For further examination of the printability of the sample exhibiting the fastest viscoelastic evolution (MgO-MCl0.1), a StoneFlower 4.0 Multimaterial four-axis 3D printer was utilized to produce ten layers of a rectangular wall, using a 7 mm diameter nozzle that extruded the paste at a speed of 20 mm/s. The findings revealed that RMC containing HA exhibited excellent buildability up to the third layer when printed (Fig. 13(a)). Nevertheless, after reaching the fifth layer, the wall structure began to experience failure, primarily evidenced by the extrusion layer collapsing towards one side (Fig. 13(b)). This could be attributed to the w/b ratio employed in this study, 0.6, which was selected to enable precise measurement of rheo-viscoelasticity. Although the introduction of HA enhanced the hydration of RMC, its yield stress or storage modulus could not meet the necessary requirements when the number of printing layers was high, ultimately resulting in paste yield and flow issues. If these pastes were to be employed for 3D printing purposes, it would be imperative to control additional variables, such as the w/b ratio, RMC reactivity, and carbonation curing conditions.

To achieve satisfactory outcomes in 3D printing, the paste must exhibit a sufficient storage modulus (yield stress) and thixotropy. The former ensures that the extruded paste can resist pressure from the upper layers without deformation; while the latter ensures that the viscosity of the paste rapidly decreases as it passes through the screw, thereby avoiding the risk of nozzle orifice blockage caused by excessive viscosity. Moving forward, it is crucial to determine how to regulate other rheological parameters to meet the workability requirements of all stages of 3D printing.

5. Conclusions

The hydration of RMC systems is limited due to the slow dissolution of MgO and the precipitation of brucite on the surfaces of MgO particles, preventing the continuation of the hydration reaction. This study aimed to investigate the evolution of the rheo-viscoelasticity of fresh RMC pastes incorporating three different hydration agents (HAs) after 3 h of hydration and establish the hydration mechanism in the presence of HAs via the use of various microscopic analyses. The following conclusions were drawn from the findings:

(1) Without HA, the G' of MgO-H_2O system increased from the order of 10^3–10^6 Pa after 3 h of hydration; whereas the *G''* increased from approximately 10^2 to 10^5 Pa. Not only did the addition of HAs substantially improve the G' and *G''* of RMC pastes at the initial stage, but also boosted their growth rate over time. $MgCl_2$ considerably enhanced the elasticity development; and the initial setting time of samples incorporating HCl and $MgCl_2$ was advanced to 100–110 min.

(2) The shear stress of MgO-H_2O and MgO-MCH0.1 grew exponentially within 3 h of hydration, whereas the shear stress of MgO-HCl0.1 and MgO-MCl0.1 peaked at 100–110 min, followed by a decline. Due to the continual tiny amplitude oscillation action of SAOS, even if the applied strain was smaller than critical strain,

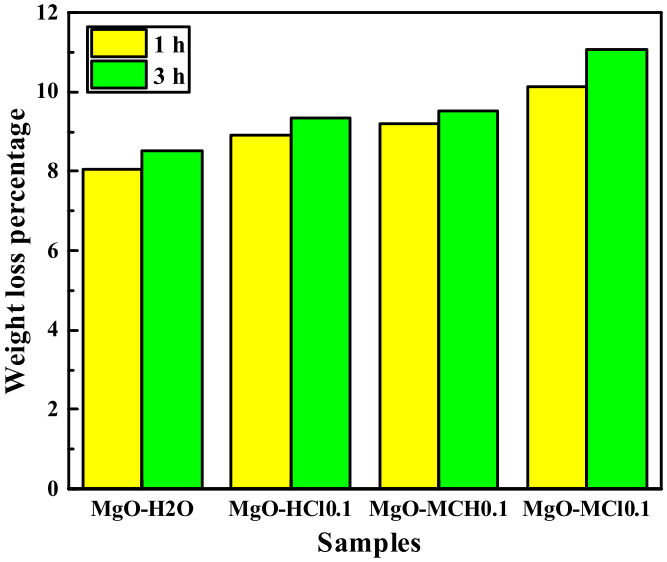

Fig. 10. mass loss of selected RMC samples in the temperature range of 300–500 °C.

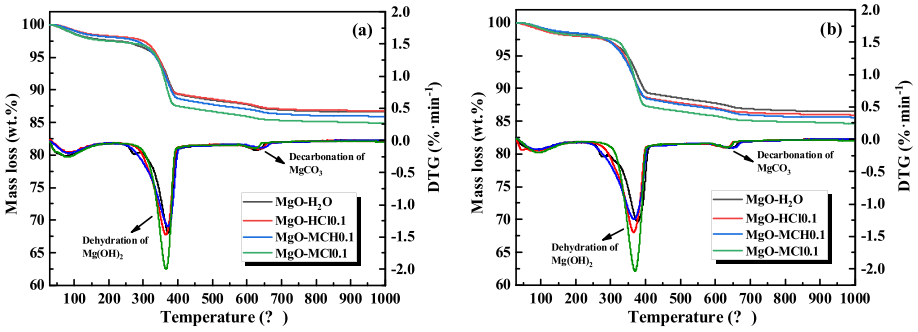

Fig. 9. TG-DTG results of fresh RMC pastes with and without HA, after: (a) 1 h and (b) 3 h.

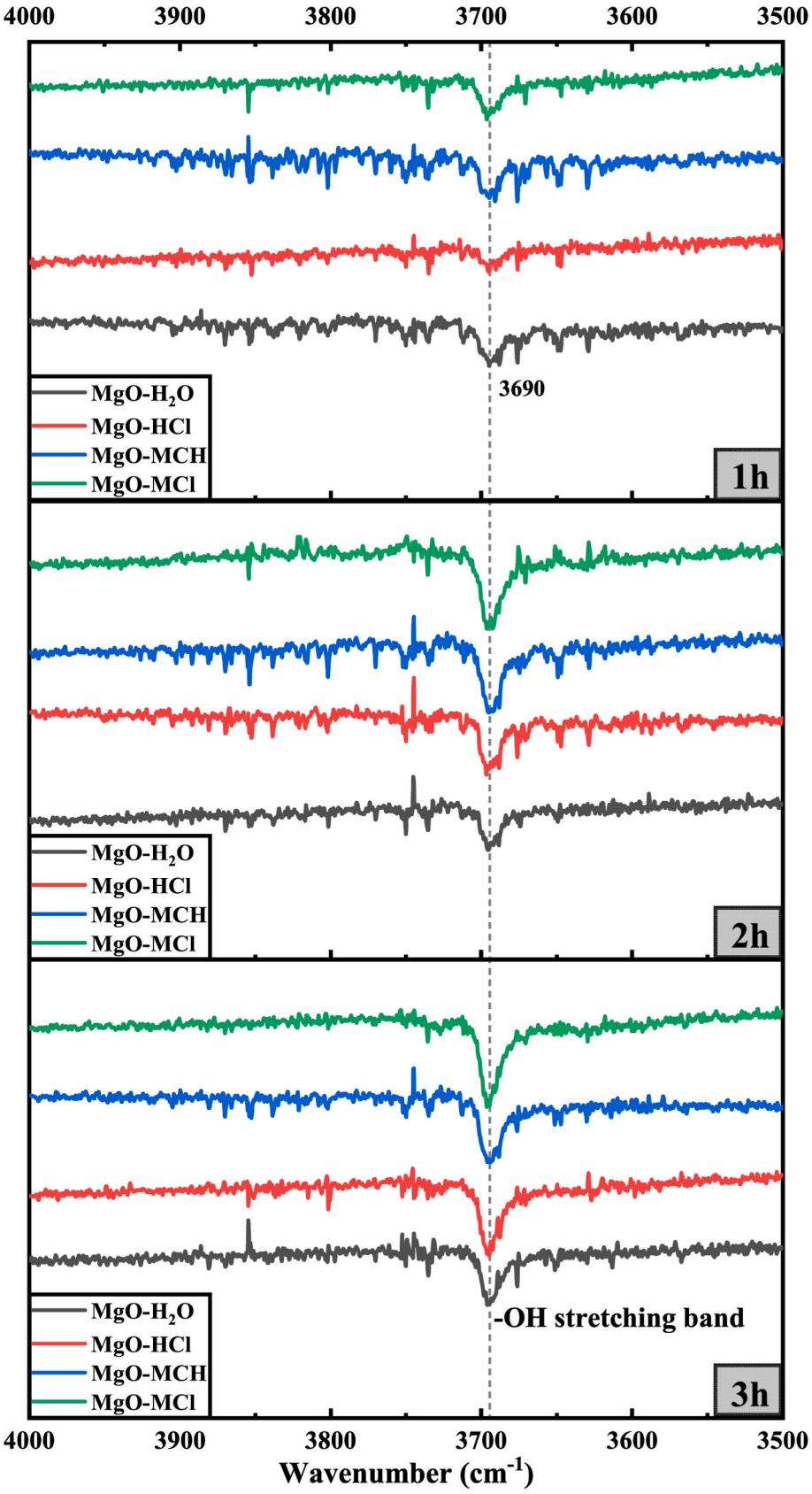

Fig. 11. FTIR spectra of fresh RMC samples at different hydration times.

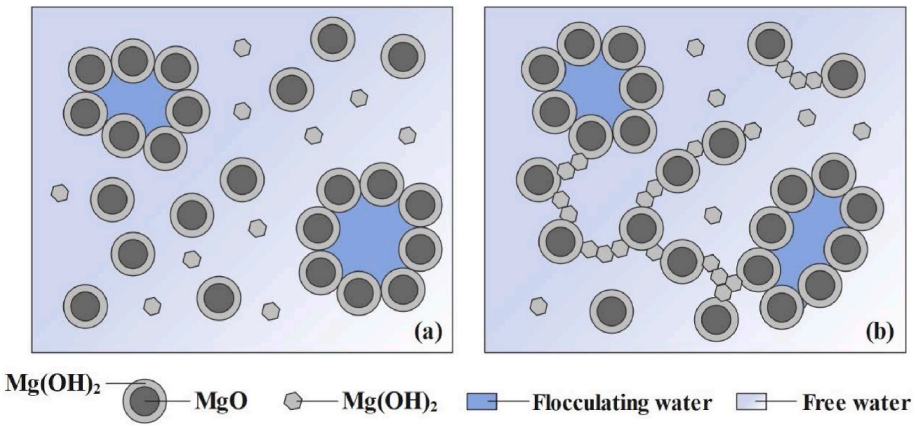

Fig. 12. Schematic illustration of fresh-state MgO-H_2O pastes, showing pastes: (a) Without HAs and (b) with HAs.

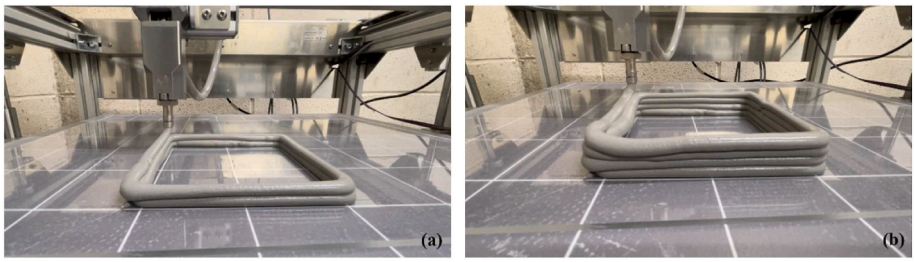

Fig. 13. Extrusion-based 3D printed component showing up to the: (a) 3rd layer and (b) 5th layer.

fatigue load action damaged the pastes after 110 min, which could account for the subsequent considerable fall in yield stress.

(3) At the same hydration period, MgO-MCH0.1 revealed the lowest pH values, whereas the control group without any HA had the highest pH, showing that the addition of HAs consumed OH^- in the suspension and promoted the formation of reaction products. Additionally, the findings of isothermal calorimetry indicated that MgO-0.1MCl released the greatest amount of hydration heat within 3 h. This finding was confirmed by XRD, TG and FTIR data, indicating the highest brucite content in the sample incorporating $MgCl_2$. Compared to the control group, the other two HAs also enhanced the early hydration of MgO-H_2O system to a certain extent.

(4) The addition of HAs in the MgO pastes enabled the brucite that was wrapped around MgO particles to progressively dissolve in the bulk solution as Mg^{2+}, raising the Mg^{2+} concentration in the suspension system. Some brucite nucleated and grew away from the reaction particles, forming a denser microscopic network structure and boosting the evolution of elasticity.

The use of HAs has been shown to significantly improve the non-destructive structural build-up of RMC systems, which can correspond to the buildability property needed during 3D printing. Furthermore, the promotion of the initial setting enabled by HAs translated into a reduced duration for the densification of paste microstructure. Overall, the findings of this study revealed the evolution of storage modulus and static yield stress with time, providing valuable new information on the understanding of the rheo-viscoelastic behavior of RMC systems at early stages. In this study, $MgCl_2$ proved to be the most efficient HA for the RMC system. Accordingly, the paste incorporating 0.1 M $MgCl_2$ displayed the most rapid G' and τ growth rate and superior printability compared to the other three mixes. This information can establish a strong foundation for more effective applications of RMC mixes in the field of 3D printing. Further investigations on establishing a balance between the extrudability, flowability and buildability of RMC mixes could facilitate the use of these binders in the development of 3D printed composites on a wider scale.

Declaration of competing interest

The authors declare that they have no known competing financial interests or personal relationships that could have appeared to influence the work reported in this paper.

Data availability

No data was used for the research described in the article.

Acknowledgements

This study was funded by the Newton Fund Institutional Links project 623812328 provided by the British Council and China Scholarship Council (grant number: 202006370082).

References

[1] S. Her, T. Park, E. Zalnezhad, S. Bae, Synthesis and characterization of cement clinker using recycled pulverized oyster and scallop shell as limestone substitutes, J. Clean. Prod. 278 (2021).
[2] Y. Peng, C. Unluer, Modeling the mechanical properties of recycled aggregate concrete using hybrid machine learning algorithms, Resour. Conserv. Recycl. 190 (2023), 106812.
[3] J. Lehne, F. Preston, Making Concrete Change, Innovation in Low-Carbon Cement and Concrete, 2018.
[4] J.L. Provis, Alkali-activated materials, Cement Concr. Res. 114 (2018) 40–48.
[5] Y. Peng, C. Unluer, Analyzing the mechanical performance of fly ash-based geopolymer concrete with different machine learning techniques, Construct. Build. Mater. 316 (2022), 125785.
[6] S.A. Walling, J.L. Provis, Magnesia-based cements: a journey of 150 Years, and cements for the future? Chem. Rev. 116 (7) (2016) 4170–4204.
[7] C. Unluer, Carbon Dioxide Sequestration in Magnesium-Based Binders, Carbon Dioxide Sequestration in Cementitious Construction Materials, 2018, pp. 129–173.
[8] K. Scrivener, F. Martirena, S. Bishnoi, S. Maity, Calcined clay limestone cements (LC3), Cement Concr. Res. 114 (2018) 49–56.

[9] C. Unluer, A. Al-Tabbaa, Impact of hydrated magnesium carbonate additives on the carbonation of reactive MgO cements, Cement Concr. Res. 54 (2013) 87–97.
[10] S. Ruan, C. Unluer, Comparative life cycle assessment of reactive MgO and Portland cement production, J. Clean. Prod. 137 (2016) 258–273.
[11] C. Unluer, A. Al-Tabbaa, Enhancing the carbonation of MgO cement porous blocks through improved curing conditions, Cement Concr. Res. 59 (2014) 55–65.
[12] N.T. Dung, A. Lesimple, R. Hay, K. Celik, C. Unluer, Formation of carbonate phases and their effect on the performance of reactive MgO cement formulations, Cement Concr. Res. 125 (2019).
[13] A.J.W. Harrison, Reactive Magnesium Oxide Cements, Google Patents, 2008.
[14] H. Dong, C. Unluer, E.-H. Yang, A. Al-Tabbaa, Recovery of reactive MgO from reject brine via the addition of NaOH, Desalination 429 (2018) 88–95.
[15] H. Dong, C. Unluer, E.-H. Yang, A. Al-Tabbaa, Synthesis of reactive MgO from reject brine via the addition of NH4OH, Hydrometallurgy 169 (2017) 165–172.
[16] C. Sonat, C. Lim, M. Liska, C. Unluer, Recycling and reuse of reactive MgO cements–A feasibility study, Construct. Build. Mater. 157 (2017) 172–181.
[17] E.G. Soares, J. Castro-Gomes, Carbonation curing influencing factors of carbonated reactive magnesia cements (CRMC)–A review, J. Clean. Prod. 305 (2021), 127210.
[18] Z. Xing, L. Bai, Y. Ma, D. Wang, M. Li, Mechanism of magnesium oxide hydration based on the multi-rate model, Materials 11 (10) (2018) 1835.
[19] N. Dung, C. Unluer, Potential additives for magnesia-based concrete with enhanced performance and propensity for CO2 sequestration, J. CO2 Util. 56 (2022), 101834.
[20] F. Jin, K. Gu, A. Al-Tabbaa, Strength and hydration properties of reactive MgO-activated ground granulated blastfurnace slag paste, Cem. Concr. Compos. 57 (2015) 8–16.
[21] N.T. Dung, R. Hay, A. Lesimple, K. Celik, C. Unluer, Influence of CO2 concentration on the performance of MgO cement mixes, Cem. Concr. Compos. 115 (2021).
[22] N.T. Dung, C. Unluer, Influence of accelerated hydration and carbonation on the performance of reactive magnesium oxiae concrete, Adv. Cement Res. 32 (2) (2020) 78–90.
[23] N.T. Dung, C. Unluer, Development of MgO concrete with enhanced hydration and carbonation mechanisms, Cement Concr. Res. 103 (2018) 160–169.
[24] R. Zhang, D.K. Panesar, Water absorption of carbonated reactive MgO concrete and its correlation with the pore structure, J. CO2 Util. 24 (2018) 350–360.
[25] N.T. Dung, C. Unluer, Performance of reactive MgO concrete under increased CO2 dissolution, Cement Concr. Res. 118 (2019) 92–101.
[26] L. Mo, F. Zhang, M. Deng, Effects of carbonation treatment on the properties of hydrated fly ash-MgO-Portland cement blends, Construct. Build. Mater. 96 (2015) 147–154.
[27] N.T. Dung, C. Unluer, Carbonated MgO concrete with improved performance: the influence of temperature and hydration agent on hydration, carbonation and strength gain, Cem. Concr. Compos. 82 (2017) 152–164.
[28] D. Filippou, N. Katiforis, N. Papassiopi, K. Adam, On the kinetics of magnesia hydration in magnesium acetate solutions, J. Chem. Technol. Biotechnol.: International Research in Process, Environmental & Clean Technology 74 (4) (1999) 322–328.
[29] K.P. Matabola, E.M. van der Merwe, C.A. Strydom, F.J. Labuschagne, The influence of hydrating agents on the hydration of industrial magnesium oxide, J. Chem. Technol. Biotechnol. 85 (12) (2010) 1569–1574.
[30] N.T. Dung, C. Unluer, Advances in the hydration of reactive MgO cement blends incorporating different magnesium carbonates, Construct. Build. Mater. 294 (2021).
[31] N. Dung, C. Unluer, Sequestration of CO2 in reactive MgO cement-based mixes with enhanced hydration mechanisms, Construct. Build. Mater. 143 (2017) 71–82.
[32] Y.M. Peng, K.L. Ma, C. Unluer, W.X. Li, S.J. Li, J.Y. Shi, G.C. Long, Method for calculating dynamic yield stress of fresh cement pastes using a coaxial cylinder system, J. Am. Ceram. Soc. 104 (11) (2021) 5557–5570.
[33] N. Roussel, Rheological requirements for printable concretes, Cement Concr. Res. 112 (2018) 76–85.
[34] B. Lu, Y. Weng, M. Li, Y. Qian, K.F. Leong, M.J. Tan, S. Qian, A systematical review of 3D printable cementitious materials, Construct. Build. Mater. 207 (2019) 477–490.
[35] F. Hamidi, F. Aslani, Additive manufacturing of cementitious composites: materials, methods, potentials, and challenges, Construct. Build. Mater. 218 (2019) 582–609.
[36] Y. Peng, K. Ma, G. Long, Y. Xie, Influence of nano-SiO2, nano-CaCO3 and nano-Al2O3 on rheological properties of cement–fly ash paste, Materials 12 (16) (2019) 2598.
[37] T. Wangler, N. Roussel, F.P. Bos, T.A.M. Salet, R.J. Flatt, Digital concrete: a review, Cement Concr. Res. 123 (2019).
[38] L. Reiter, T. Wangler, N. Roussel, R.J. Flatt, The role of early age structural build-up in digital fabrication with concrete, Cement Concr. Res. 112 (2018) 86–95.
[39] Y. Zhang, Y. Zhang, W. She, L. Yang, G. Liu, Y. Yang, Rheological and harden properties of the high-thixotropy 3D printing concrete, Construct. Build. Mater. 201 (2019) 278–285.
[40] A. Douba, S. Ma, S. Kawashima, Rheology of fresh cement pastes modified with nanoclay-coated cements, Cem. Concr. Compos. 125 (2022), 104301.
[41] Y. Peng, C. Unluer, Development of alternative cementitious binders for 3D printing applications: a critical review of progress, advantages and challenges, Compos. B Eng. (2022), 110492.
[42] A. Khalil, X. Wang, K. Celik, 3D printable magnesium oxide concrete: towards sustainable modern architecture, Addit. Manuf. 33 (2020).
[43] B. Panda, C. Sonat, E.-H. Yang, M.J. Tan, C. Unluer, Use of magnesium-silicate-hydrate (M-S-H) cement mixes in 3D printing applications, Cem. Concr. Compos. 117 (2021).
[44] S. Kumar, J. Lei, E.-H. Yang, C. Unluer, Influence of different additives on the rheology and microstructural development of MgO–SiO2 mixes, Compos. B Eng. 235 (2022), 109784.
[45] A.W. Saak, H.M. Jennings, S.P. Shah, The influence of wall slip on yield stress and viscoelastic measurements of cement paste, Cement Concr. Res. 31 (2) (2001) 205–212.
[46] A. Poulesquen, F. Frizon, D. Lambertin, Rheological behavior of alkali-activated metakaolin during geopolymerization, J. Non-Cryst. Solids 357 (21) (2011) 3565–3571.
[47] J.T. Kolawole, R. Combrinck, W.P. Boshoff, Rheo-viscoelastic behaviour of fresh cement-based materials: cement paste, mortar and concrete, Construct. Build. Mater. 248 (2020), 118667.
[48] J.T. Kolawole, R. Combrinck, W.P. Boshoff, Shear rheo-viscoelasticity approach to the plastic cracking of early-age concrete, Cement Concr. Res. 135 (2020), 106127.
[49] Z. Sun, T. Voigt, S.P. Shah, Rheometric and ultrasonic investigations of viscoelastic properties of fresh Portland cement pastes, Cement Concr. Res. 36 (2) (2006) 278–287.
[50] T. Huang, Q. Yuan, F. He, Y. Xie, Understanding the mechanisms behind the time-dependent viscoelasticity of fresh C3A–gypsum paste, Cement Concr. Res. 133 (2020), 106084.
[51] Q. Yuan, X. Lu, K.H. Khayat, D. Feys, C. Shi, Small amplitude oscillatory shear technique to evaluate structural build-up of cement paste, Mater. Struct. 50 (2) (2017) 1–12.
[52] Q. Yuan, D. Zhou, K.H. Khayat, D. Feys, C. Shi, On the measurement of evolution of structural build-up of cement paste with time by static yield stress test vs. small amplitude oscillatory shear test, Cement Concr. Res. 99 (2017) 183–189.
[53] T. Zhang, C. Cheeseman, L. Vandeperre, Development of low pH cement systems forming magnesium silicate hydrate (MSH), Cement Concr. Res. 41 (4) (2011) 439–442.
[54] K. Li, Y. Wang, N. Yao, A. Zhang, Recent progress of magnesium oxychloride cement: manufacture, curing, structure and performance, Construct. Build. Mater. 255 (2020).
[55] G. Jauffret, J. Morrison, F. Glasser, On the thermal decomposition of nesquehonite, J. Therm. Anal. Calorim. 122 (2) (2015) 601–609.
[56] N. Roussel, G. Ovarlez, S. Garrault, C. Brumaud, The origins of thixotropy of fresh cement pastes, Cement Concr. Res. 42 (1) (2012) 148–157.
[57] A. Perrot, D. Rangeard, A. Pierre, Structural built-up of cement-based materials used for 3D-printing extrusion techniques, Mater. Struct. 49 (4) (2015) 1213–1220.
[58] Y. Qian, S. Kawashima, Distinguishing dynamic and static yield stress of fresh cement mortars through thixotropy, Cem. Concr. Compos. 86 (2018) 288–296.